

Distribution Agreement

In presenting this thesis as a partial fulfillment of the requirements for a degree from Emory University, I hereby grant to Emory University and its agents the non-exclusive license to archive, make accessible, and display my thesis in whole or in part in all forms of media, now or hereafter now, including display on the World Wide Web. I understand that I may select some access restrictions as part of the online submission of this thesis. I retain all ownership rights to the copyright of the thesis. I also retain the right to use in future works (such as articles or books) all or part of this thesis.

Jessica Fahim
10, 2024

April

The Cloning, Expression, and Purification of α -CA Nanobody for HIV-1 Capsid Assays

by

Jessica Fahim

Stefan Sarafianos, PhD
Adviser

Biology

Stefan Sarafianos, PhD
Adviser

Edward Nam, PhD
Committee Member

Leila Rieder, PhD
Committee Member

2024

The Cloning, Expression, and Purification of α -CA Nanobody for HIV-1 Capsid Assays

By

Jessica Fahim

Stefan Sarafianos, PhD

Adviser

An abstract of
a thesis submitted to the Faculty of Emory College of Arts and Sciences
of Emory University in partial fulfillment
of the requirements of the degree of
Bachelor of Science with Honors

Biology

2024

Abstract

The Cloning, Expression, and Purification of α -CA Nanobody for HIV-1 Capsid Assays

By Jessica Fahim

In the face of escalating global infectious disease threats, there is a growing imperative to advance diagnostic tools for early detection and treatment. Monoclonal antibodies (mABs), though pivotal for infectious disease detection and treatment, are hindered by their sizable nature, susceptibility to denaturation, and dependence on post-translational modifications, imposing constraints on their production and purification. Nanobodies, compact antibody fragments derived from Camelids, present a promising solution by overcoming the limitations of mABs. Their diminutive size and single-domain structure enable swift production in *E. coli* and an increased ability to detect biomarkers with exceptional sensitivity. The binding of the previously reported nanobody '59H10' to the C-terminal domain of the HIV-1 Capsid protein (CA).¹² To obtain an α -CA nanobody for HIV-1 capsid assays, an expression system was generated by cloning for the 59H10 nanobody. The coding sequence of the 59H10 nanobody was amplified using polymerase chain reaction and subsequently inserted into the pET24a vector by Gibson assembly, yielding the 59H10 expression vector with diverse functional tags. Following transformation into NiCo21 (DE3) competent *E. coli*, the vector was sequenced to validate successful cloning. A construct of the nanobody with a 6x Histidine tag was purified from *E. coli* by a nickel column. The specificity and affinity of the nanobody was tested *via* biolayer interferometry. Our interest in 59H10 is due to the reported use of the α -CA nanobodies in stabilizing and solubilizing CA_{SpyCat} (or CA_{SpyTag}) modular capsid assembly system from Summers et al. (2019).¹³ The lab also has an interest in using this as a tool in future experiments for investigating HIV-1 capsid biochemistry.

The Cloning, Expression, and Purification of α -CA Nanobody for HIV-1 Capsid Assays

By

Jessica Fahim

Stefan Sarfianos, PhD

Adviser

A thesis submitted to the Faculty of Emory College of Arts and Sciences
of Emory University in partial fulfillment
of the requirements of the degree of
Bachelor of Science with Honors

Biology

2024

Acknowledgements

My thanks to William McFadden, my mentor, who supported me and has helped me grow as a scientist and an individual. This thesis could not have been completed without him. I would also like to thank Dr. Stefan Sarafianos for giving me the opportunity to work in his research lab with such amazing and intelligent people. I would also like to thank Zachary Lorson and Andres Emanuelli who have been so helpful throughout my project and have taken time out of their busy schedules to guide me. In addition to my other committee members, Dr. Leila Rieder and Dr. Edward Nam, were very supportive throughout this project, for which I am grateful.

This project was funded by R01 AI120860, F31 AI174951, and U54 AI170855 grants.

Table of Contents

Chapter 1: Introduction.....	1
HIV-1 Structure and Mechanism of Entry.....	1
Figure 1.....	2
Figure 2.....	4
Figure 3.....	5
Figure 4.....	7
Nanobody vs. Monoclonal Antibodies (mABs).....	8
Figure 5 & 6.....	10
Molecular Binding of 59H10.....	11
Chapter 2: Materials and Methods.....	14
Cloning of the 59H10 nanobody in pET24a.....	14
Figure 7.....	15
Figure 8.....	16
Protein Expression and Purification of 59H10:6xHis.....	20
HIV-1 CA121 Expression.....	22
Biotinylating 59H10 nanobody for Bio-Layer Interferometry (BLI).....	23
Chapter 3: Results.....	25
Cloning of the 59H10 nanobody.....	25
Figure 9.....	26
Figure 10.....	27
59H10:6xHis Expression and Purification.....	28
Figure 11.....	29
Figure 12.....	30

Figure 13.....	33
Figure 14.....	34
Figure 15.....	35
BLI of 59H10 and HIV-CA121.....	36
Figure 16.....	37
Figure 17.....	38
Figure 18.....	39
Chapter 4: Discussion.....	41
Chapter 5: Figures.....	43
Chapter 6: References.....	46

Introduction

Human Immunodeficiency Virus (HIV-1) remains a global health crisis, impacting over 38.4 million individuals worldwide as of 2021 (figure 1).²⁰ In East and South Africa alone, approximately 20.6 million individuals are affected by HIV, underscoring the regional burden of the virus.²⁰ The prevalence of this virus not only highlights its substantial impact on public health but also emphasizes the urgent need for ongoing and intensified research efforts. The sheer magnitude of those affected underscores the gravity of the situation, requiring a comprehensive and multifaceted approach to combat the challenges presented by the HIV-1 pandemic. HIV-1, a member of the lentivirus family, possesses a distinctive capability to infect CD4⁺ human immune cells. This distinctive trait emphasizes the tendency of the virus to target critical components of the human immune system. As the virus infiltrates and replicates within CD4⁺ cells, it instigates the development of Acquired Immune Deficiency Syndrome (AIDS) when untreated.¹ This advanced stage of the infection signifies a profound compromise of the immune system, rendering individuals susceptible to opportunistic infections and malignancies. The progression to AIDS underscores the severity of the health crisis and accentuates the need for innovative approach in treatment and prevention.

HIV-1 Structure and Mechanism of Entry

The potency and widespread prevalence of HIV-1 can be attributed to several key factors that make it a formidable pathogen. Despite how small the genome is (approximately 10 kilobase pairs), HIV-1 displays a remarkable ability to adapt and mutate rapidly, creating diverse viral strains.² As a retrovirus, HIV-1 takes advantage of host cell components while being able to evade the immune system. HIV-1 initiates its entry by binding to a CD4 receptor and CCR5 and

Human Immunodeficiency Virus (HIV) Impact 2021

38.4 million people
are living with HIV

650,000 deaths
from AIDS-related illnesses

1.5 million infections
were newly established



Source: UNAIDS 2021 Estimates

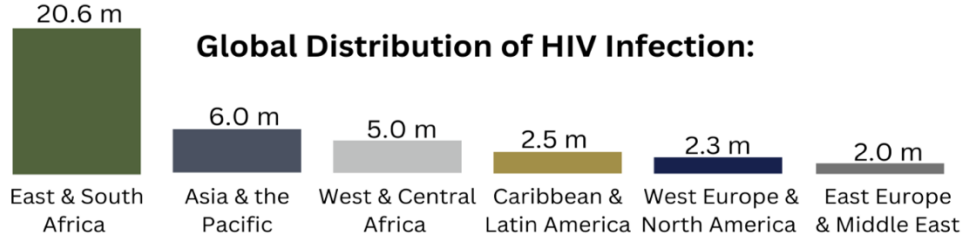


Figure 1: UNAIDS 2021 Estimates reveal the continued burden of HIV/AIDS worldwide, with 38.4 million people living with HIV, 650,000 deaths from AIDS-related illnesses, and 1.5 million new infections.²⁰ Regional distribution indicates the highest prevalence in East and South Africa (20.5 million), followed by Asia and the Pacific (6 million), West and Central Africa (5 million), the Caribbean and Latin America (2.3 million), and East Europe and the Middle East (2.0 million). Created with BioRender.com

CXCR4 coreceptors.³ Following attachment is the fusion event, a critical step in HIV -1 infection. The viral capsid is released into the host cell. This viral core consists of capsid proteins that are assembled and house two positive sense RNA strands and cell components that are necessary for genome integration into the host genome.¹ Reverse transcriptase, a necessary component carried in the viral capsid, is an enzyme that allows for the conversion of the viral RNA genome into complementary DNA. This process is known as reverse transcription. Because there is no proofreading mechanism in this process, this leads to mutations that allow for diverse variants and genetic diversity, aiding the virus in its infectivity of future host cells.⁴ After the viral genome has undergone reverse transcription to form the cDNA, it now needs to be integrated into the host cell's chromosomal DNA. This integration process is facilitated by integrase, a viral enzyme that facilitates this process. Integrase and the viral DNA form a preintegration complex (PIC) that is transported into the nucleus and the viral DNA is integrated, or incorporated, into the host cell's chromosomal DNA.⁵ Integrase acts by cleaving the host cell's genomic DNA and ligating the viral DNA into the host genome. This integration allows the viral genetic material to become a permanent part of the host cell's DNA, where it can be transcribed and translated along with the host's own genes. Following integration, the integrated viral DNA is termed a provirus, representing the permanent incorporation of HIV-1 genetic material into the host genome (figure 2). The provirus is used as the template for the transcription of new viral RNA that are used to create viral proteins or become a part of a new virus. The provirus can also be transcriptionally inactive in the latent stage. This allows the virus to evade the host immune response, because there is no viral RNA or proteins being actively produced.¹

HIV Replication Cycle

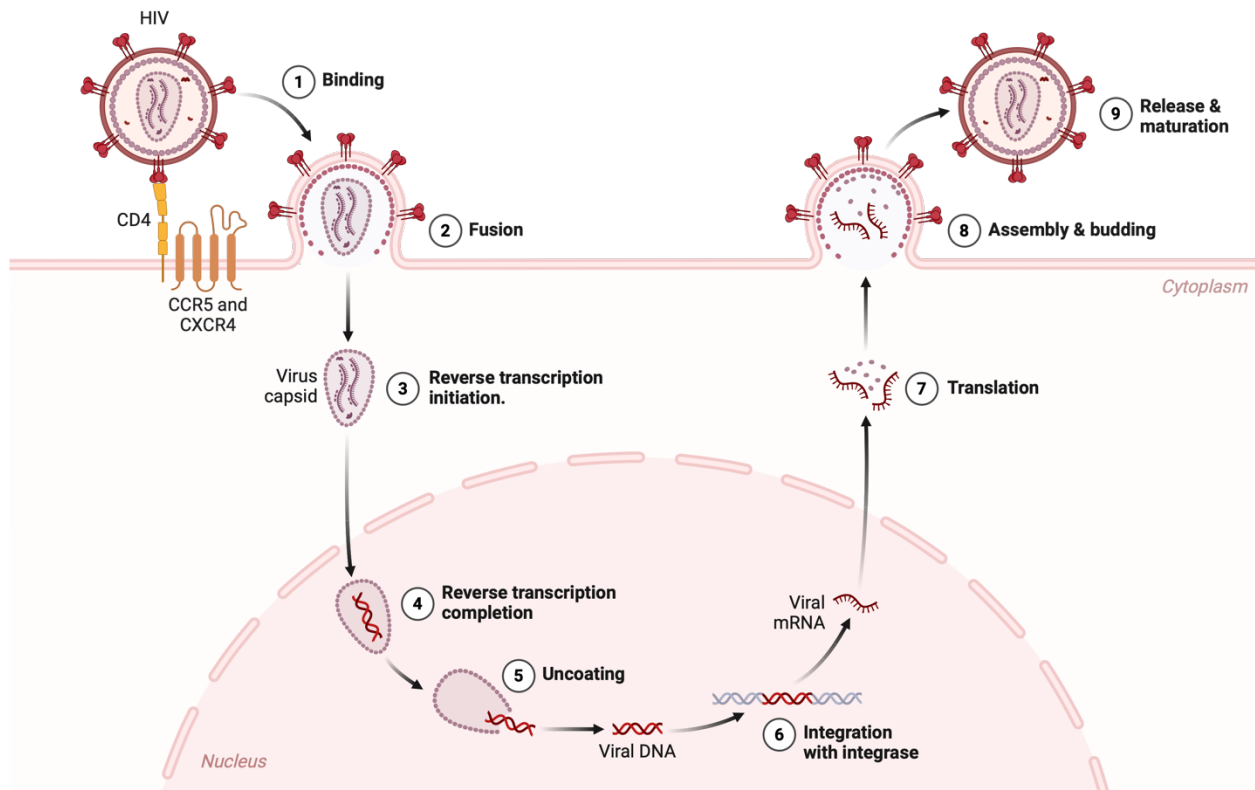


Figure 2: The HIV replication cycle depicts key stages in viral propagation. The process is initiated with the virus binding to CD4 receptor and co-receptors CCR5 and CXCR4, followed by fusion and reverse transcription within the viral capsid (CA). Subsequent stages include uncoating, integration with the host genome via integrase, translation, assembly, budding, release and maturation, contributing to the viral life cycle and pathogenesis. Made with BioRender.com

HIV-1 virion

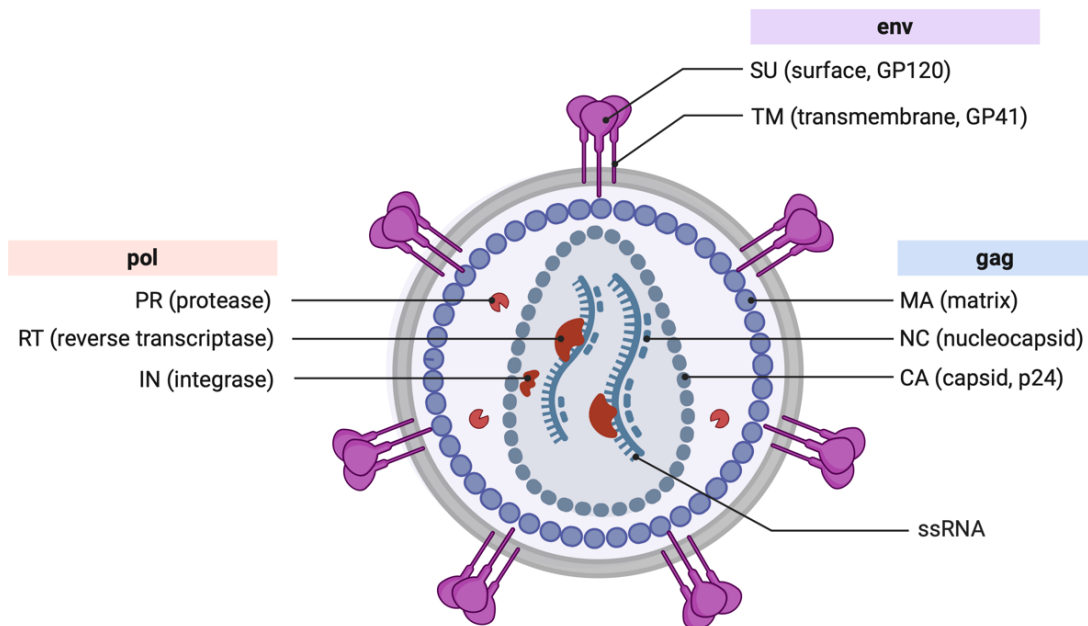


Figure 3: The HIV-1 virion structure illustrates components crucial for viral replication and pathogenesis. The viral particle consists of structural proteins encoded by gag (matrix, nucleocapsid, and capsid), enzymes encoded by pol (protease, reverse transcriptase, and integrase), and envelope glycoproteins encoded by env (surface GP120 and transmembrane GP41). Additionally, the single-stranded RNA (ssRNA) genome serves as the genetic blueprint for viral replication. Made with BioRender.com

The structure of HIV encompasses a lipid envelope containing glycoproteins like gp120 and gp41. These glycoproteins facilitate the virus's interaction with the host cell during entry through binding to the CD4 receptors on the host cell.⁶ Within the lipid envelope is the capsid, a protein shell in the shape of a fullerene cone formed by approximately 1500 capsid proteins (CA).⁷ This structure serves as a critical protective role, encapsulating and safeguarding the genetic material (figure 3). In addition to shielding RNA during the early stages of infection, the capsid plays a pivotal role in the subsequent steps of the viral replication cycle. CA has important roles during and after reverse transcription; the process of reverse transcription converting the viral RNA genome into double-stranded DNA occurs within the capsid to prevent the exposure of viral nucleic acid to host proteins. While not fully understood, there are several speculative functions of CA in the role of reverse transcription. Firstly, the capsid acts as a molecular reaction vessel, containing the polymerase enzyme, RT, and other elements within the core during the discontinuous process of reverse transcription.¹⁰ Numerous studies have implicated that the HIV-1 capsid interacts with host proteins to conceal the viral DNA from cytoplasmic DNA sensors.¹⁰ Mutants with unstable capsids experience the degradation of viral RNA and viral proteins, showing the importance of capsid stability in the viral process.¹⁰

The CA protein in the HIV capsid has two parts: the N-terminal domain (CA_{NTD}) and the C-terminal domain (CA_{CTD}).¹⁸ In the mature CA, such as CA121, the formation of N-terminal domain (CA_{NTD}) to C-terminal domain (CA_{CTD}) interactions occurs within the hexameric structure, followed by inter-hexamer interactions involving both CA_{NTD} - CA_{NTD} and CA_{CTD} - CA_{CTD} interactions.⁸ Hexamers refer to the structures composed of six CA protein subunits. In the capsid assembly process, CA proteins come together to create hexameric subunits, where each hexamer consists

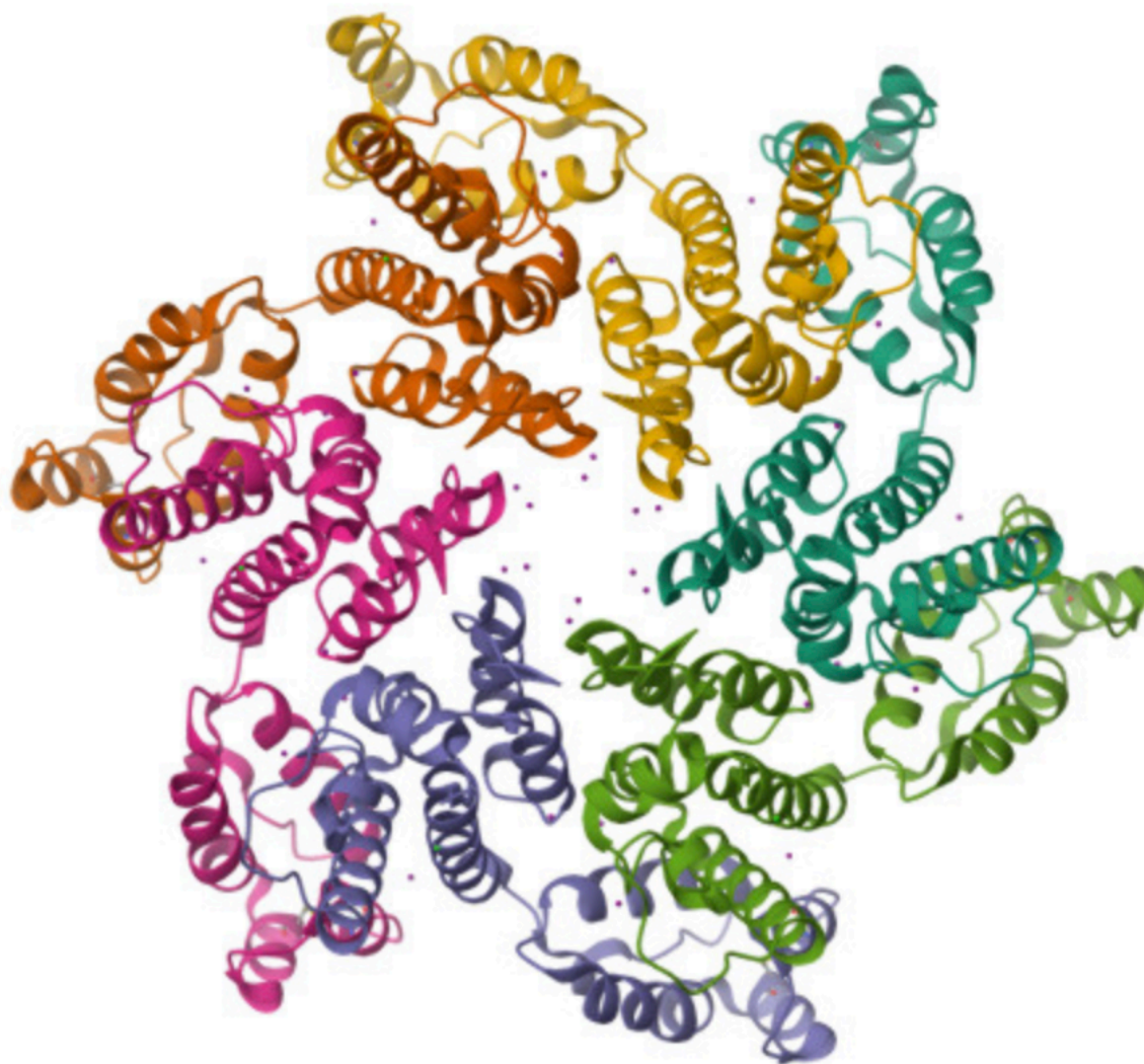


Figure 4: The structure of a capsid hexamer, as revealed by PDB entry 4XFX, demonstrates the assembly of capsid proteins.¹⁸ Each distinct color represents a capsid protein within the hexamer assembly.

of six individual CA proteins arranged in a specific pattern (figure 4). About 250 hexameric subunits and 12 pentamers make an enclosed fullerene-cone observed in a mature virus.¹ These subunits play a role in the stability of the capsid assembly. The N-terminal domain of the CA protein, with its seven α -helices, plays a stabilizing role in these hexameric subunits. Hexamers, along with pentameric subunits, collectively form the fullerene cone-shaped capsid. The orientation and arrangement of these hexamers and pentamers contribute to the unique arrangement of the capsid, which is essential for its protective function during various stages of the viral life cycle.

The significance of the capsid in the viral life cycle of HIV underscores the importance of targeting and studying these components for both therapeutic and research purposes.

Therapeutically, disrupting the stability or assembly of hexamers and the capsid is considered a promising strategy for inhibiting HIV replication.¹⁹ By targeting these essential structures, researchers aim to interfere with key stages of the viral life cycle, potentially leading to the development of novel antiviral treatments. *In vitro* studies often rely on stabilized forms of hexameric capsid structures. Having soluble capsid hexamer interactions for *in vitro* studies offers an advantage by providing manageable systems, enabling the investigation of hexamer-hexamer interfaces within a small, functionally relevant portion of the HIV capsid core, which addresses the challenges associated with larger capsid structures in biochemical assays.

Nanobody vs. Monoclonal Antibodies (mABs)

Monoclonal antibodies (mABs) have become indispensable tools in biological assays, renowned for their exceptional specificity in detecting target molecules. Comprising four peptide chains, these antibodies are meticulously engineered to recognize and bind to specific epitopes with high affinity. However, their widespread use is accompanied by significant challenges,

primarily stemming from their intricate structure, which necessitates substantial post-translational modifications. The production and purification of monoclonal antibodies can be resource-intensive, imposing limitations on scalability and efficiency.¹⁷ Specific to HIV, a limitation also arises from the inherent challenge antibodies face when trying to access the interior of cells. While antibodies are highly specific and stable molecules that can recognize and bind to particular target molecules, their size and structure make it difficult for them to cross the cell membrane.⁹ As of 2021, there were 49 HIV medicines approved by the FDA.¹ These medicines are lifesaving and have had a tremendous effect on millions of people all around the world. Because of the challenges these medicines have faced, such as toxicity and drug resistance, it is crucial to continue to create novel antivirals that can help diagnostically and therapeutically.

Nanobodies originate from the single-chain antibody fragments in Camelid immunoglobulins. In mABs, the variable domains consist of both heavy and light chains, with the heavy chain variable domain (VH) and the light chain variable domain (VL) contributing to antigen recognition. This dual-chain structure in mABs provides a diverse repertoire of specificities. Traditional mABs weigh around, 150 kDa, which can hinder their ability to access certain epitopes.¹¹ On the other hand, nanobodies are characterized by a single-chain variable domain (VHH). Nanobodies are derived from heavy chain antibodies found in Camelids. While traditional antibodies consist of two heavy and two light chains, heavy chain antibodies lack the light chain, resulting in a smaller size and simpler structure (figure 5). The heavy chain in nanobodies plays a pivotal role as the sole contributor to antigen binding. This single-domain structure streamlines the antibody's composition, making nanobodies smaller and more

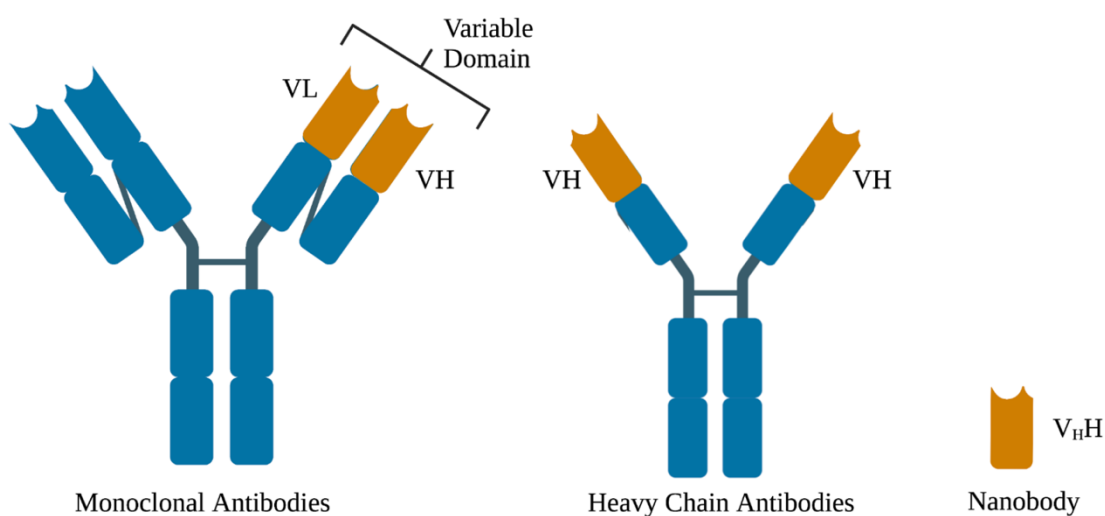


Figure 5: A size comparison of monoclonal antibodies, heavy chain antibodies, and nanobodies exhibit conventional structures with both heavy and light chains, while heavy chain antibodies contain only heavy chains, labeled VH. Made with BioRender.com

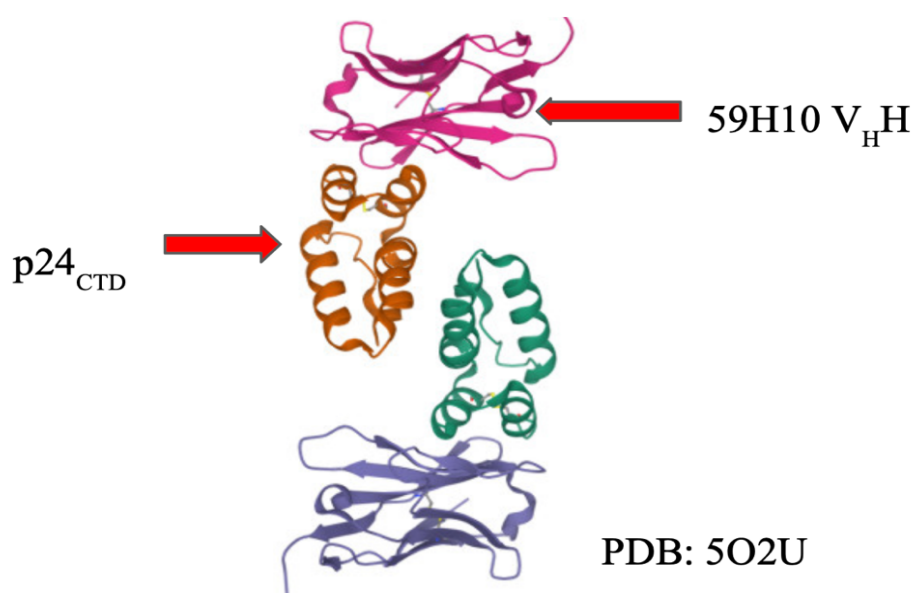


Figure 6: Visualization of the binding interaction between the CA_{CTD} (capsid C-terminal domain) and the 59H10 nanobody (PDB 5O2U).¹² The CA_{CTD} is depicted in orange and green, while the nanobody is illustrated in pink and purple.

straightforward, compared to mABs. The absence of a light chain in nanobodies simplifies their design and production while retaining a high affinity and specificity. This distinction in variable domain composition contributes to the unique features and advantages of nanobodies in various applications. Nanobodies are approximately 11-15 kDa, making them ten times smaller than mABs (figure 5).¹¹ Nanobodies have hydrophilic surfaces which enables nanobodies to solubilize dimers and multimers, such as the HIV-1 hexamers.¹¹ In addition, there has been research that nanobodies can withstand environments with extreme pH and high temperatures.¹¹ The production in *E. coli* offers advantages such as its single-chain construction and absence of post-translational modifications, which expedites the production process significantly.¹¹ The smaller size of the nanobody provides an advantage as a tool in biomarker interactions. Overall, their small size and unique structure make nanobodies advantageous for accessing specific epitopes, providing new avenues for therapeutic and diagnostic applications in the context of HIV-1.

Molecular Binding of 59H10

The molecular dynamics of nanobody 59H10 showcase a robust specific interaction with HIV-1 capsid protein, demonstrating high affinity and stability. This strong interaction is attributed to the R50 to CA E213 interaction. This is facilitated by multiple hydrogen bond pairs forming between arginine and glutamate residues, allowing for up to four interactions at an optimal orientation of amino acids (figure 6).¹² Moreover, Gray et al. (2017) tested a panel of sequences of the VHH single-chain domain that was obtained from two HIV-1 CA immunized llamas. The panel was evaluated through CA binding affinity assays to obtain nanobodies that detected a large range of HIV-1 strains and subtypes. They reported nanobodies (59H10 and 37E7) that effectively target HIV-1 capsid protein (CA) with high specificity. Through the inoculation of the llamas with target antigen, RNA was extracted and the VHH domain was

sequenced and cloned. To obtain the DNA sequences of the nanobodies, RNA is reverse transcribed, and PCR amplified, resulting in DNA sequences. The nanobodies (59H10 and 37E7) were analyzed to find the molecular binding site of each nanobody to CA. Through sequence characterization of 59H10 and 37E7, the nanobodies contrast at 3 amino acid sites. Binding of the 59H10 nanobody occurs at helix 10 and helix 11 at the C-terminal of CA (CA_{CTD}) between residues R50 and E213 respectively. This interaction has a dissociation constant (K_D) of about 300 nM. In addition, hydrogen bonds are formed between W37 and A205, N32 and Q219, R50 and both P207 and L205 respectively. The mutation 59H10 W37 also has hydrophobic interaction with CA. The 37E7 nanobody binds to CA similarly to 59H10-CA complex varying only at the 37E7 Y56 residue.

In addition to identifying biomarkers with high sensitivity, the nanobody is an effective tool in preventing aggregate prone CA lattice. The lower affinity nanobody 37E7 was reported to stabilize and solubilize CA_{SpyCat} (or CA_{SpyTag}) modular capsid assembly system from Summers et al. (2019). The SpyCatcher system is a protein engineering method that is used to establish stable connections between different components of the HIV capsid. It involves two components: SpyCatcher and SpyTag. SpyCatcher is a beta-barrel protein that is derived from *Streptococcus pyogenes*, while SpyTag is 13 amino acid polypeptide. When mixed, they link through an isopeptide bond between specific side chains.¹⁴ This creates a robust linkage which can be used to facilitate the stabilization and attachment of complex protein components. In the case of HIV, this SpyCatcher system was employed to stably link multiple hexamers in a capsid lattice arrangement, aiding in the study of host factors binding to the HIV capsid.¹³

The CA nanobody binds to the CA_{CTD}, blocking inter-hexameric interactions of CA. This could interfere with Gag assembly. By introducing SpyCatcher and SpyTag into CA constructs,

large hepta-hexamer assemblies were formed. However, they tended to aggregate and precipitate, posing purification challenges. When an anti-capsid nanobody with an affinity to CA was introduced into the mix, it would prevent non-specific aggregation.¹³ This resulted in soluble hepta-hexamers, offering a valuable tool for studying host factors targeting large capsid regions. Although not the goal of this project, when co-expressed with HIV-1 infected cells, 59H10 nanobody decreases the infectivity of HIV-1 virus produced to 32% of wild-type.¹⁶

The overarching goal of the project is to clone, purify, and characterize the 59H10 nanobody, which targets the capsid protein of HIV-1. By focusing on the CA hexamer assembly, the project aims to maintain biological relevance of the capsid protein, which naturally forms hexameric structures in the virus. Preserving the structural integrity of the CA proteins in its hexameric form ensures accurate representation of its physiological state, including its quaternary structure and conformational epitopes crucial for interaction with other. Molecules like nanobodies. This approach prevents potential disruptions caused by truncating the protein, which could alter its binding properties and compromise the accuracy of binding affinity measurements. This assembly of complexes between CA hexamer and 59H10 nanobody allows for the detailed characterization of the complexes, offering valuable insights on their interactions and potential applications in combating HIV-1 infection.

Materials and Methods

Cloning of the 59H10 nanobody in pET24a

The plasmid vector pET24-a-VHH-mCherry (addgene plasmid #109421) a pET24a vector backbone with a vector size of 6452 base pairs (figure 7). The tags and fusion proteins include T7 (N terminal), HA (C terminal), BAP (C terminal), and His6 (C terminal).¹⁵ These tags are important for both the purification and expression process. In addition, the plasmid contains the GFP nanobody, and mCherry fluorescence gene, and a kanamycin resistance gene. Two different constructs were engineered. The first construct incorporated the 59H10 nanobody sequence along with furoin tags, including mCherry, HA (a common antibody epitope), and AviTag (59H10:mCherry:HA:Avi). The second construct was devoid of these additional elements. It solely comprised of the 59H10 nanobody sequence with a 6x His Tag (59H10:6xHis). To create the 59H10 expression vectors, Gibson Assembly, a process that utilizes overlapping ends, exonuclease, polymerase, and ligase, was used to create the recombinant 59H10 vector (figure 8). The 59H10 sequence was obtained from the reported structure Gray et al. (2017), codon optimized for expression in *E. coli*, and purchased from GenScript. To amplify the cDNA, Polymerase Chain Reaction (PCR) was used with the appropriate primers. In this process, two specific forward and reverse primers (WM12_F, WM14_R, WM24_F, WM26_R) engineered with overhangs, allowing them to be integrated into the pET24-a-VHH-mCherry vector after digestion (table 1). WM12_F and WM14_R were used for the 59H10:mCherry construct while WM24_F and WM26_R was used for the 59H10:6xHis construct. The PCR reaction included the designed primers, cDNA (59H10 sequence), 2x NEB Phusion mix, and deionized water (dH₂O). Primers were purchased and synthesized by IDT. In the controls of the experiment, the first control was a primer-only control to ensure there was no

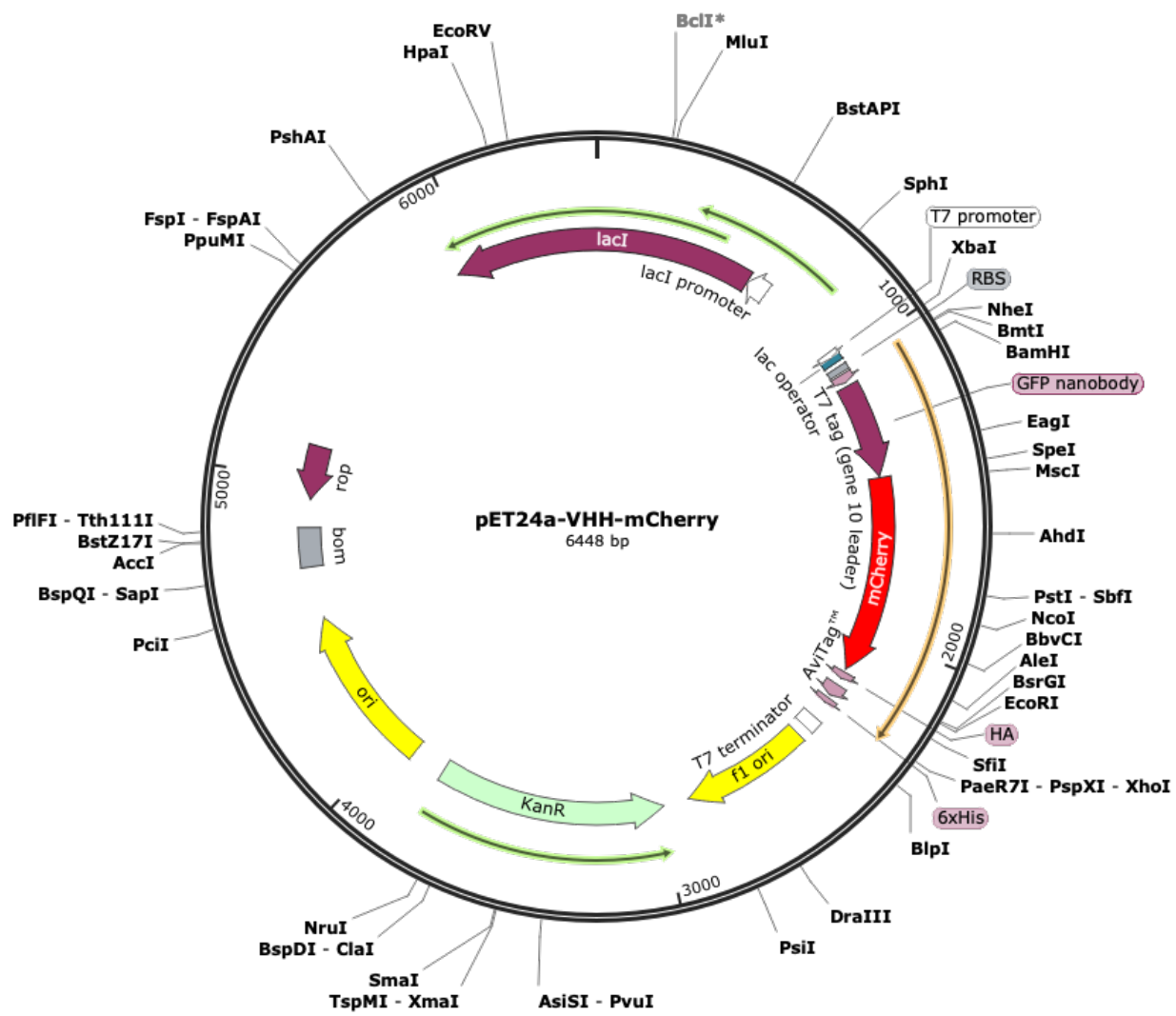


Figure 7: Plasmid vector map of the pET24a-VHH-mCherry plasmid (Addgene plasmid #109421).¹⁵ The plasmid contains the GFP nanobody, mCherry fluorescence gene, HA tag, and 6xHis tag. Map created with Snapgene V. 6.0.6.



Figure 8: Schematic representation of engineered expression constructs derived from the pET24-a-VHH-mCherry plasmid vector (Addgene plasmid #109421). (A) Original pET24-a-VHH-mCherry construct featuring mCherry fluorescence gene and tags/fusion proteins including T7 (N-terminal), HA (C-terminal), BAP (C-terminal), and His6 (C-terminal). (B) First engineered construct incorporating the 59H10 nanobody sequence with a 6x His Tag. (C). The construct incorporating the 59H10 nanobody with tags: mCherry, HA, and AviTag.

primer dimer formation nor contaminating DNA (table 2 & 3). These dimers may interfere with the amplification process of the 59H10 sequence. In addition, contaminated DNA may lead to false-positive results, as the amplification could be due to the unintended presence of DNA in the reaction mix. The experimental group contained 1.25 μL of both primers, 0.5 μL of the 59H10 sequence, 12.5 μL of the (HF) NEB Phusion mix and 9.5 μL of dH_2O to a total of 25 μL . The primer control had the same amount of primer and (HF) NEB Phusion mix, 10 μL of dH_2O , and no cDNA. Finally, the cDNA control had no primer, 0.5 μL of cDNA, 12.5 of the (HF) NEB Phusion mix and 12 μL of dH_2O (table 2). The thermocycler settings can be found in table 3, with the annealing steps being repeated 30 times.

Restriction digestion, involving the enzymes BamHI and SpeI (NEB), was utilized to remove the α -GFP nanobody (VHH) from the plasmid (pET24-a-VHH-mCherry) (table 4). BamHI recognizes the DNA sequence 5'-G'GATCC-3', cleaving between the first two G's, while SpeI recognizes 5'-A'CTAGT-3', cleaving between the A and the first C. The process involves incubating the plasmid DNA with these enzymes, leading to the cleavage of the pET24a vector to remove VHH. Two single digest controls involve treating the plasmid DNA with each enzyme individually - one control for BamHI and another for SpeI. By doing so, we are able to determine whether each enzyme performs its intended functions. An uncut control is crucial for ruling out the possibility of contamination or unexpected enzymatic activity that could compromise the integrity of the experimental results, as well as a comparison point. The enzymes BamHI and SpeI were used for the 59H10:mCherry:HA:Avi construct. NheI enzyme recognizes 5'-G'CTAGC-3', cleaving between the first G and C, while XhoI recognizes 5'-CTCGAG-3', cleaving between the first C and T. These enzymes were used for the 59H10:6xHis

construct (figure 10). Approximately 5 μg of the plasmid was added in each group except for the uncut control. These were left to incubate overnight in a 37°C water bath.

In a process of preparing a 1% agarose gel for DNA fragment analysis, a solution was created by combining 75 mL of 1X Tris-Acetate-EDTA (TAE) buffer with 0.75 grams of agarose powder (Bio-Helix). After thorough mixing, the solution was heated until the agarose completely dissolved. Subsequently, 6x loading dye was added to the cooled agarose solution to aid in visualizing the DNA migration during electrophoresis. The gel was poured into a casting tray, and upon solidification, the comb was removed to form wells for sample loading. Gel electrophoresis was performed by placing the gel in an electrophoresis chamber filled with 1X TAE buffer, and DNA samples, mixed with loading dye, were loaded into the wells. An electric current was applied to facilitate DNA migration based on size. The gel was stained with ethidium bromide and visualized under UV light using the Azure Biosystems 600 gel documentation system (figure 9).

Following the completion of both the restriction digestion and the PCR product analysis on a 1% agarose gel, the desired DNA fragments were carefully excised from the gel. The gel extraction process was carried out using QIAGEN gel extraction kit. In this procedure, the excised gel slices containing the specific DNA fragments were subjected to QIAGEN's proprietary technology for efficient DNA purification. The gel slices were treated to remove contaminants, including agarose, and the purified DNA was then eluted using 40 μL of elution buffer. This step ensured the concentration and purity of the extracted DNA, making it suitable for subsequent molecular biology applications.

The Gibson Assembly reaction was then conducted by combining the purified fragments with a Gibson Assembly master mix containing DNA polymerase with exonuclease activity and

DNA ligase. After gel extraction of both the insert and vector, the assembly was carried out using NEB HiFi Assembly with varying amounts and ratios. To maximize yield and efficiency, two ratios were employed: 1:1 and 1:3 insert to vector. Additionally, a control ratio of 1:0 was included to assess the self-ligation capability of the vector. Since bacterial cells are only capable of replicating circular DNA, the presence of colonies in the 1:0 ratio indicates successful self-ligation of the vector alone. If both the 1:1 and the 1:0 ratios yield similar colony counts, it suggests that the insert was not effectively added. However, if the 1:1 ratio results in a higher number of colonies compared to the 1:0 ratio, it indicates the successful insertion of the 59H10 PCR product into the digested vector (table 5).

After assembling the expression vector, bacterial transformation was conducted to introduce these vectors into bacterial cells. First, the expression vectors were transformed in XL1 Blue competent cells for cloning and plasmid propagation. XL1 Blue *E. coli* cells are commonly used for cloning due to their high transformation efficiency and the presence of the lacZ Δ M15 marker. Once the plasmid constructs were confirmed and purified from XL1 Blue cells by midiprep, they were transformed into NiCo21 DE3 cells for protein expression. NiCo21 DE3 *E. coli* cells are specifically engineered for high-level expression of recombinant proteins and carry the T7 RNA polymerase gene under the control of the lacUV5 promoter, allowing for tight regulation of gene expression using IPTG induction. The transformation process involves combining the assembly mixes with XL1 Blue competent cells in a volume of 50 μ L and incubating on ice for 30 minutes. This is followed by a brief heat shock treatment of 45 seconds in 42°C water bath to facilitate the uptake of the plasmid by the cells. Subsequently, the transformed cells are incubated in 1 mL of LB media without antibiotic in a shaker at 37°C for an hour. The cells are then plated on agar plates containing kanamycin, and only cells that

successfully take up the plasmid and express the kanamycin resistance gene will survive and form colonies on these plates, while untransformed cells will not. The plated cells are then left to grow overnight in a 37°C incubator.

After bacterial expression, the harvested bacterial pellets containing the expressed proteins were subjected to plasmid DNA extraction using the QIAGEN Midi Prep kit. The bacterial pellet was resuspended in a lysis buffer containing lysozyme and RNase to break down the bacterial cell wall and degrade RNA. Next, the lysate was loaded onto a Midi column, where plasmid DNA selectively bind to the silica membrane of the column while other cellular debris and contaminants are washed away. Finally, the bound plasmid was eluted with 0.2 mL of elution buffer.

Protein Expression and Purification of 59H10:6xHis

An 8-liter batch of LB broth supplemented with kanamycin was prepared and 10 mL aliquots of the stock culture containing the recombinant vector expressed in NiCo21 DE3 cells were inoculated into the broth. The culture was then transferred to a New Brunswick Innova 44R shaking incubator set at a 37°C. Periodic measurements of the optical density at 600 nm (OD₆₀₀) were taken using a spectrophotometer to monitor the growth of the bacterial culture. A blank consisting of LB broth with kanamycin only was also measured to establish a baseline reading. Once the culture reached an optical density around 0.4, indicating that the cells were in exponential growth phase, 400 µL of isopropyl β-D-1-thiogalactopyranoside (IPTG) was added to the culture to induce protein expression. The induction process was carefully monitored to ensure optimal protein expression levels. Subsequent measurements of OD₆₀₀ and sample collection were performed at specific time points to track cell growth and assess protein expression levels. After induction with IPTG, the batches were left in the shaker at 16°C to allow

for overnight protein expression. Following incubation, the bacterial cultures were harvested by centrifugation at 15,000xg for 30 minutes at 4°C. The resulting pellet contains the bacterial cells with the desired nanobody; a growth curve was graphed (figure 11).

A 4-20% gradient gel for SDS-PAGE (Sodium Dodecyl Sulfate Polyacrylamide Gel Electrophoresis) analysis, was purchased from Bio-Rad. The gel was stained with Coomassie blue G250. Before loading the samples onto the gel, protein samples were prepared by mixing them with a sample buffer containing SDS and β -mercaptoethanol and boiled at 95°C for 10 minutes. This denatures the proteins and gives them a negative charge proportional to their size, allowing for separation based primarily on molecular weight. The gel was then imaged using Azure Biosystems 600 (figure 12).

The bacterial pellets were thawed and then resuspended in 30 mL of phosphate-buffered saline (PBS) supplemented with 20 mM imidazole, 200 μ g/mL lysozyme, 20 μ g/mL DNase I, 1 mM PMSF, incubated for 10 minutes at room temperature followed by 1 hour incubation on ice to prepare for lysis. Lysis continued through a tip sonicator, which was operated through three cycles of sonication, each lasting 30 seconds, with cooling intervals of 1 minute in between. In total, the sonicator was operated for a total of 3 minutes, excluding the 1-minute cooling periods between each cycle of sonication. The lysate was pelleted by centrifugation at 15,000xg for 1 hour at 4°C.

The elution buffer, comprising 500 mM of imidazole (approximately 0.851 g in 25 mL of PBS), was prepared. Subsequently, 2 mL of elution buffer was diluted with 48 mL of dH₂O to achieve a final concentration of 20 mM imidazole. A low concentration of imidazole is used in the was buffer in order to disrupt weak interactions between non-specifically bound molecules and the resin while allowing the nanobody to remain bound. The supernatant containing the

59H10 nanobody was subjected to purification via a nickel column due to the presence of a 6xHis tag. Prior to loading the supernatant, the column was equilibrated with 20 mL of wash buffer. After loading the supernatant, the column was washed with an additional 20 mL of wash buffer. Finally, the elution step was carried out using 2 mL of elution buffer. The HiPrep 26/10 Desalting Column (Cytiva) was connected to the ÄKTA system, facilitating desalting and buffer exchange (figure 16). After the desalting process was complete, the eluted fractions containing the purified samples were collected and analyzed via SDS-PAGE (figure 14 & 15).

HIV-1 CA121 Expression

Initially, the HIV-CA is expressed in BL21 DE3 RIL and pelleted. The cell pellet is resuspended in lysis buffer (50 mM Tris-HCl pH 8, 50 mM NaCl, 100 mM BME) and kept on ice. After incubation and lysis using a homogenizer or sonication, the lysate is centrifuged, and the supernatant is filtered. The CA protein is then precipitated with saturated ammonium sulfate, followed by centrifugation and resuspension in lysis buffer. Dialysis into Mono Q Buffer A (25 mM Tris pH 8.1, 20 mM β ME) is performed overnight, and the supernatant is loaded onto Mono Q columns for purification via FPLC. The fractions containing HIV-CA are combined, and the process is repeated with SP Buffer A (25 mM MES pH 5.5, 20 mM BME) for further purification using SP columns. After concentrating the protein to at least 10 mg/mL, it was dialyzed against 2 L of 50 mM Tris, 2 M NaCl and 50 mM BME, pH 8.0, overnight, causing the protein to precipitate. Subsequently, it was dialyzed against 2L of 50 mM Tris, 2 M NaCl, 0.2 mM BME, pH 8, overnight. It was further dialyzed against 2L of 20 mM Tris, 40 mM NaCl, pH 8 overnight, resulting in the disappearance of the precipitate. The crosslinked hexamer formation was confirmed via SDS-PAGE gel.

Biotinylating 59H10 nanobody for Bio-Layer Interferometry (BLI)

Biotinylation for Bio-Layer Interferometry (BLI) utilized with Octet® BLI Discovery program (version 13.0.0.17, Sartorius), involves attaching biotin molecules to the nanobody. Biotin binds strongly to streptavidin, which is coated on BLI sensors. This allows for the specific and reversible immobilization of proteins on the sensor surface, enabling the study of biomolecular interactions in real-time. To calculate the amount of Sulfo-NHSC-LC-Biotin required for a 20-fold molar excess, the following formula is applied: mL of protein sample multiplied by the protein concentration in mg/mL, then multiplied by the inverse of the molecular weight in kilodaltons. This result is then multiplied by 20 to achieve the desired molar excess of biotin. This is then multiplied by 557 mg/mmol of Biotin and multiplied by 181.82 to get the amount of Biotin solution. When considering the 59H10 nanobody, the sample concentration was 2.904 mg/mL with a molecular weight of 13.09 kDa. This resulted in 309.45 µL of biotin solution. Once combined, the mixture was incubated on ice for two hours. The Thermo Scientific Zeba Spin Desalting column was inserted into a 15 mL collecting tube. The column was centrifuged at 1000xg for 2 minutes to remove the storage buffer. The side of the column where the resin was slanted upward was marked for reference. The column was equilibrated with 2.5 mL of PBS to the top of the resin bed and centrifuged at 1000xg for 2 minutes. This was repeated 3 times. The biotinylated sample was then added. And centrifuged for 1000xg for 2 minutes. A 3 kDa filter was employed to exchange the buffer from PBS to Tris. Centrifugation at 13,000 rpm for 2 minutes was performed 3-4 times to separate the buffer from the protein and exchange it with Tris buffer.

To perform the BLI assay, the first column of wells contained buffer for equilibration (20 mM Tris pH 8.2, 40 mM NaCl, 0.05% Tween 20).²¹ This was done for 120 seconds. The second

column contained 1.201 mg/mL of nanobody with the third well as a blank. This was run for 660 seconds. The third column was three wells of buffer again for equilibration, which was done for 120 seconds as well. The fourth well contained 25 μ L of 12.7 mg/mL of hexamer with the first well as a blank, which was run for 50 seconds. Finally, the last column was buffer for dissociation of the hexamer from the nanobody, which was run for 100 seconds. The first control involves the nanobody only (row A), which serves as a baseline to be subtracted from the absorbance reading of the experimental group. The second control, the hexamer only control (row C), is implemented to verify that the hexamer does not bind to the sensor (figure 18). Kinetic analyses were obtained (table 6).

The BLI assay involves measuring changes in wavelength as molecules bind to the sensor surface. Initially, a baseline measurement wavelength is established with the sensor. When the nanobody is introduced into the solution, binding to the sensor surface causes a shift in wavelength due to interference patterns being altered as light bounces off the nanobody. Subsequently, when the hexamer binds to the nanobody, there is another shift in wavelength. Finally, during dissociation, as the hexamer separates from the nanobody, there is a decrease in the shift. The data obtained from the BLI assay were analyzed kinetically to understand the binding and dissociation kinetics between the nanobody and the hexamer, providing insights into their interaction dynamics (figure 16).

Results

Cloning of the 59H10 Nanobody

To confirm the successful amplification of the 59H10 sequence via PCR, gel electrophoresis was employed for size characterization. The amplified 59H10 sequence was expected to be 342 base pairs long with the primers WM24_F and WM26_R. Upon examination of the gel image, the observed band aligned closely with the 300 bp marker of the DNA ladder (figure 9), indicating that the PCR product corresponded to the desired sequence. Notably, the absence of any bands in the primer control suggested the absence of primer dimers or DNA contamination. Similarly, the presence of a band at approximately 300 base pairs in the DNA control indicated the absence of any contamination.

Furthermore, the digestion of the pVHH vector with the enzymes NheI and XhoI was anticipated to yield a fragment size of 5,233 base pairs, considering the original vector was 6475 base pairs in length and the enzymes cleaved the GFP coding sequence, mCherry coding sequence, the HA tag, and the AviTag, all totaling 1,215 base pairs. Gel electrophoresis of the experimental DNA band revealed a faint alignment between the 5,000 base pair and the 6,000 base pair DNA ladder marker, consistent with the expected size of the digestion product. The inclusion of single digest controls further corroborated the reliability of the enzymatic digestion process. The bacterial plate colonies resulting from the transformation of the recombinant vectors into NiCo21 DE3 competent cells exhibited consistency with the expected outcomes, indicating successful cloning. To verify the fidelity of the constructed vectors, both constructs were sequenced by full-plasmid sequencing (PlasmidSaurus) to ensure structure integrity of the vectors, affirming the absence of any unexpected mutations or genetic aberrations. Both constructs were also subjected to BLAST sequencing analysis which confirmed the presence of

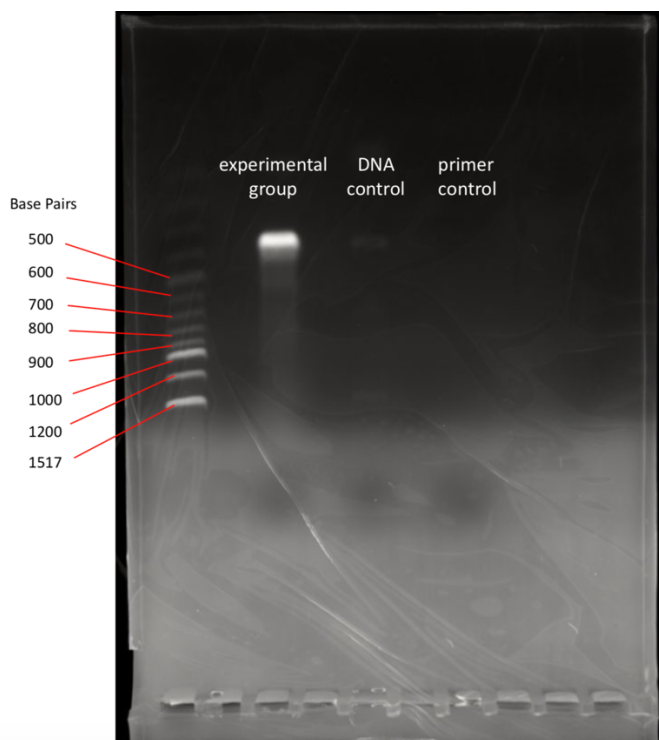


Figure 9: Gel electrophoreses image illustrating the PCR amplification of the 59H10 sequence, targeting a desired product size of 342 base pairs. Gel visualization using Azure Biosystems 600. The experimental group (amplified with primers WM24 and WM26) displays a bright band below the 500 basepair ladder marker, indicating successful amplification of the target sequence. The DNA control exhibits a faint, unamplified band, while the primer control shows no visible bands. 100 bp DNA Ladder was used from New England Biolabs.

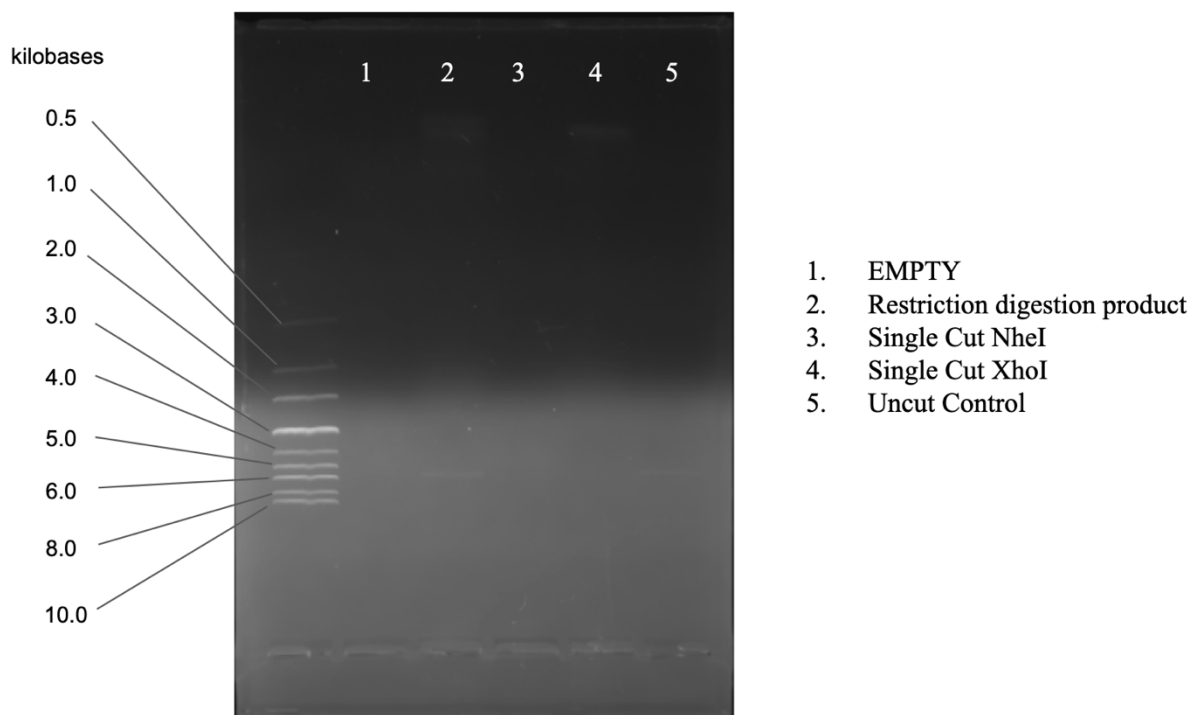


Figure 10: Gel electrophoreses of a 1% agarose gel depicting the results of restriction digest, where the restriction digest column displays a faint band between the 5 and 6 kilobase ladder markers. However, the single cut columns exhibit no visible bands. The uncut sample also reveals a faint band around 6 kilobases. Imaged with Azure Biosystems 600. 1kb DNA Ladder from New England Biolabs was used.

the intended genetic sequences and validated their identity. Collectively, these confirmatory methods provided robust validation of the successful construction of the desired vectors.

59H10:6xHis Expression and Purification

The rest of the project used the 59H10:6xHis construct for purification and Biotinylation Interferometry (BLI.) The bacterial growth curve serves as a crucial indicator for successful bacterial growth, illustrating the exponential increase in *E. coli* population over time. The bacteria were kept at 37°C for a total of 4 hours before being kept at 16°C overnight. As the bacteria proliferate, the optical density (OD) of the culture increases, reflecting the density of viable bacterial cells within the culture medium. The growth curve exhibits a lag phase, followed by exponential growth, and eventually reaches a stationary phase as nutrients become depleted or waste accumulates (figure 11). In conjunction with the growth curve analysis, the reducing SDS-PAGE of bacterial lysates provides further insights into the expression of our target protein. Following induction with IPTG, which triggers the expression of the 59H10 nanobody, we observed a distinct change in the SDS-Page banding pattern. Specifically a darker band emerged at the expected molecular range corresponding to our target protein, which has a molecular weight of 13.09 kDa. This darker band indicates the successful expression of the nanobody following induction, as the increased protein concentration results in more intense staining on the gel. The position of the dark band seems to be between 10 and 15 kDa when compared to the protein ladder, indicating that the nanobody was expressed (figure 12).

Nickel columns play a role in isolating proteins tagged with histidine. These columns exploit the high affinity between immobilized nickel ions on the column matrix and the His-tagged nanobody. The nanobody tagged with 6xHis tag is first loaded onto the column. As it

59H10 Nanobody Expression and Bacterial Growth: OD₆₀₀ Trends

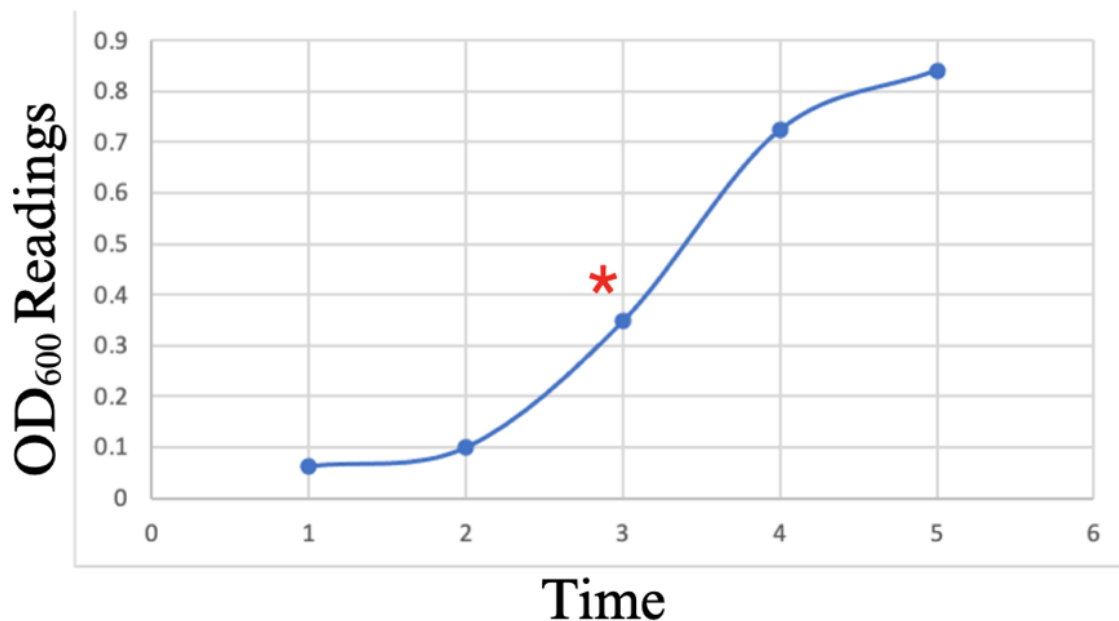
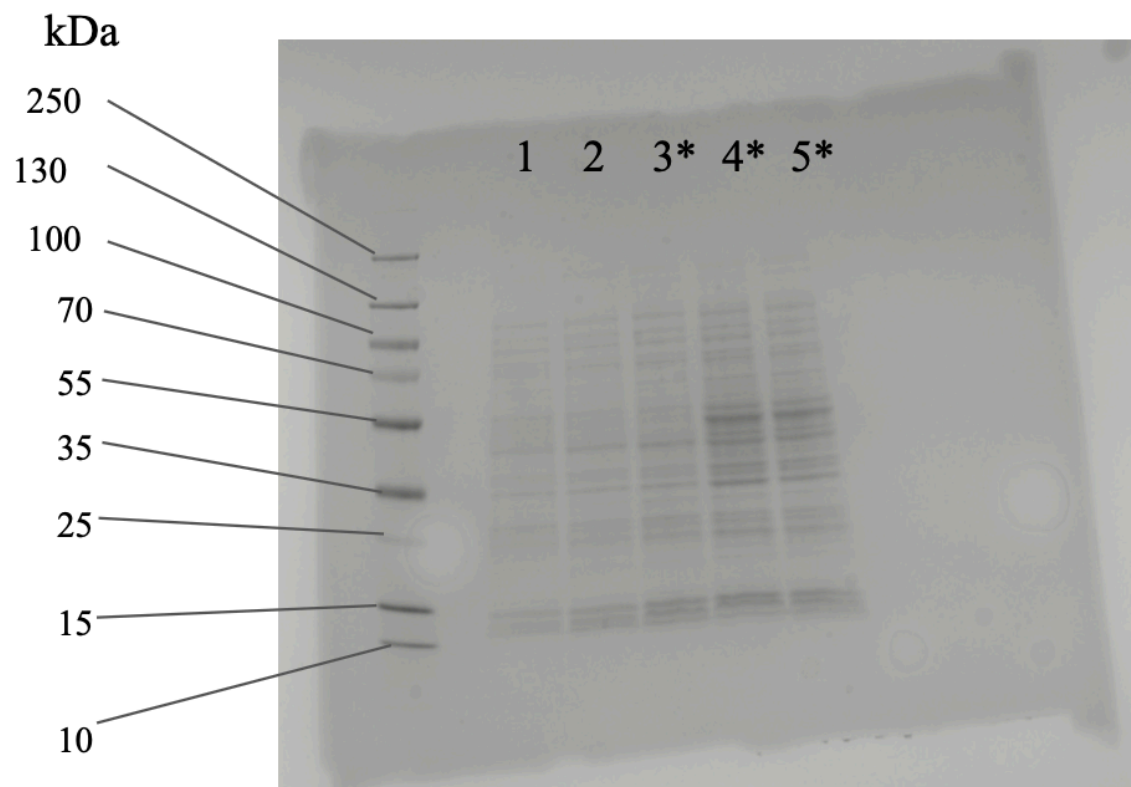


Figure 11: Growth curve illustrating the relationship between time and OD₆₀₀ readings during bacterial culture. The bacteria were kept at 37°C for a total of 4 hours before being kept at 16°C overnight. Induction with 0.4 mM of IPTG (which induces the transcription via the Lac operon) took place at time 3 (indicated by *). OD₆₀₀ readings were recorded at various time points: 0.08 at time 1, 0.1 at time 2, 0.35 at time 3, 0.72 at time 4, and 0.85 at time 5.



* = Induction

Figure 12: Image of a reducing SDS-PAGE gel with a 4-20% gradient, stained with Coomassie blue, captured using the Azure Biosystems 600 gel imaging system. The gel image displays protein bands before and after induction with IPTG, with induction initiated at time 3. Darker bands are observed post-induction. Notably, the nanobody has a molecular weight of 13.09 kDa. Color Prestained Protein Ladder from New England Biolabs was used.

flows through, proteins lacking His tags pass through, while those with His tags bind to the nickel ions. Subsequent washing steps remove nonspecifically bound proteins and contaminants, enhancing the purity of the target protein. Elution is then achieved using a buffer containing imidazole which competes with the His tag for binding to the nickel ions, thereby releasing the purified protein. During the nickel column purification process, multiple samples were collected at different stages to assess the efficiency of protein purification. The first sample was obtained from the cell pellet following bacterial expression. Upon analysis using a 4-20% gradient gel for a reducing SDS-PAGE, a distinct dark band was observed between the 10 and 17 kDa, corresponding to the expected size of the 59H10 nanobody (13.09 kDa). This initial observation indicated the presence of the expressed protein in the bacterial lysate. Subsequently, a sample was taken after lysing the cells with lysis buffer. In this sample, the darker band corresponding to the target 59H10 protein remained prominent, indicating successful extraction of the protein from the bacterial cells. The third sample was collected after equilibrating the nickel column, where no protein bands were detected as expected, confirming the absence of contaminating proteins. The next sample was the protein sample added to the column after lysing with both the lysis buffer and the sonicator. There is a distinct dark band between 10-17 kDa. Following the addition of the protein sample to the column, a subsequent sample was taken after washing with wash buffer. In this sample, no protein bands were observed, indicating the effective removal of non-specific bound material from the column matrix. Finally, the eluted protein fraction was collected, and upon analysis, a single prominent band within the 10-17kDa range was observed. This band represented the purified 59H10:6xHis nanobody and served as evidence of successful purification using the nickel column. The progressive disappearance of non-specific bands and the presence of a single purified band in the elution fraction validated the effectiveness of the

nickel column purification process in isolating the target protein from the bacterial lysate (figure 13).

Following the nickel column purification step, desalting was performed using the ÄKTA Pure system. Desalting following nickel column gel filtration involves the removal of imidazole and other low-molecular-weight compounds from the eluted protein sample. This process is done by passing the protein solution through a desalting column, selectively retaining the nanobody while allowing small molecules (imidazole) to be removed. The desalting process was monitored using UV recording, with the blue line on the graph representing the absorbance of the nanobody at a specific wavelength. UV monitoring was employed during desalting to track the absorbance of the nanobody at specific wavelengths, enabling real-time assessment of the protein concentration. Notable, the blue line appeared prominently between collecting columns A8 through B2, suggesting successful desalting and purification of the 59H10 nanobody (figure 15). To confirm the identity of the purified protein, fractions A4, A9-B4, B10, C9, and D4 were collected post-desalting and subjected to SDS-Page analysis using a reducing 4-20% gradient gel (figure 14). Remarkably, fraction A9 through B1 exhibited a distinct band corresponding to the expected molecular weight range of the nanobody, which is approximately 10-17 kDa, as indicated by the protein ladder. This observation strongly suggests the presence of the 13.09 kDa 59H10 nanobody in the desalted fractions. To further validate these findings, the sample collected before desalting was also loaded onto the gel for comparison. The analysis revealed a similar band pattern between fractions A9 through B1 affirming that the desalting process effectively purified the nanobody from contaminants. Consequently, the desalted fractions containing the purified nanobody were identified, providing a high degree of confidence in the purity and integrity of the isolated protein.

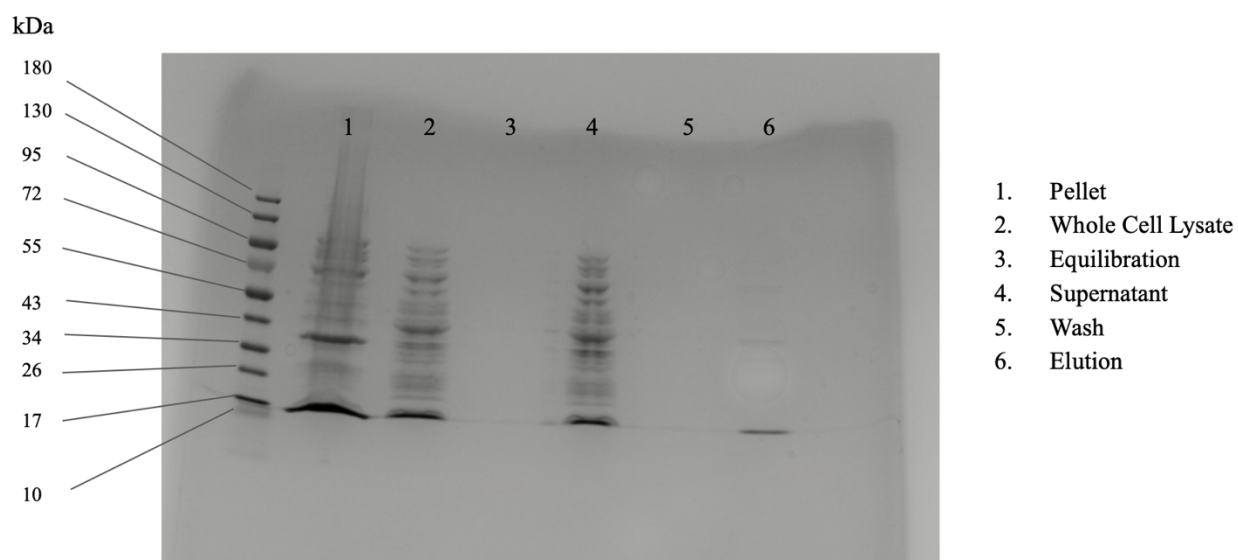


Figure 13: Image of a reducing SDS-PAGE with a 4-20% gradient stained with Coomassie blue, captured on the Azure Biosystems 600 gel imaging system. The gel depicts various stages of the protein purification process of the 59H10:6xHis construct. The first column represents the pelleted sample after bacterial induction, displaying a distinct bright band between 10 and 17 kDa. Whole cell lysate, the supernatant after pelleting down post-bacterial induction, still shows the presence of the bright bands. Equilibration of the nickel column with wash buffer results in the absence of bands. The supernatant after incubation in lysis buffer and sonication reveals protein band with the bright band persisting between 17 and 10 kDa. Washing the nickel column resulted in no visible bands. The final column displays only the band between 10 and 17 kDa after elution from the nickel column. The 59H10 nanobody construct was expected to be 13.09 kDa. Color Prestained Protein Ladder from New England Biolabs was used.

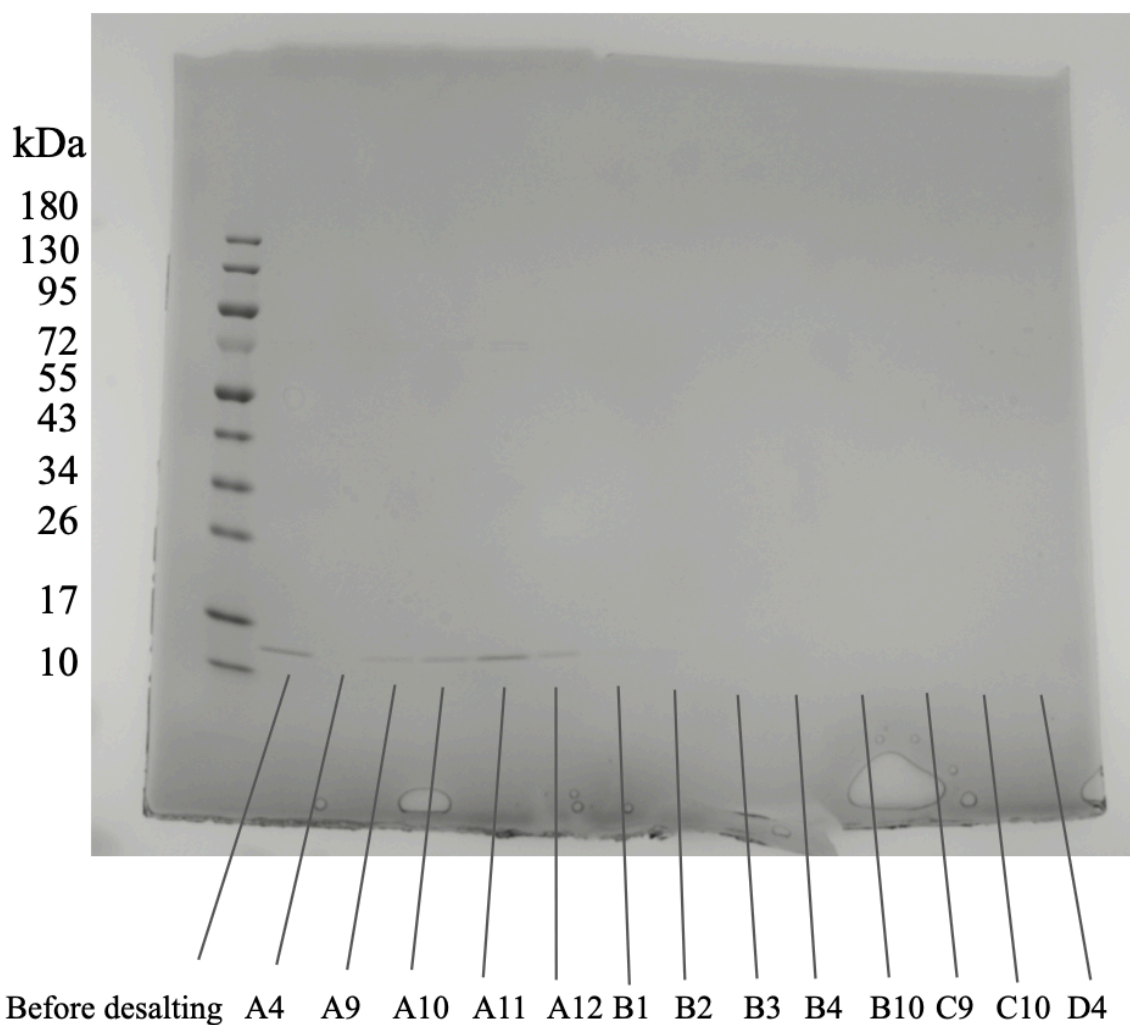


Figure 14: Image of a reducing SDS-PAGE with a 4-20% gradient stained with Coomassie blue, captured using the Azure Biosystems 600 gel imaging system. The samples were collected after desalting with the ÄKTA Pure desalting column. Samples were taken from A4, A9-B4, B10, C9, C10, and D4, with bands appearing at A9-B1 between 10-17 kDa. The first column is the sample added before desalting, also showing a band between 10-17 kDa. Color Prestained Protein Ladder from New England Biolabs was used.

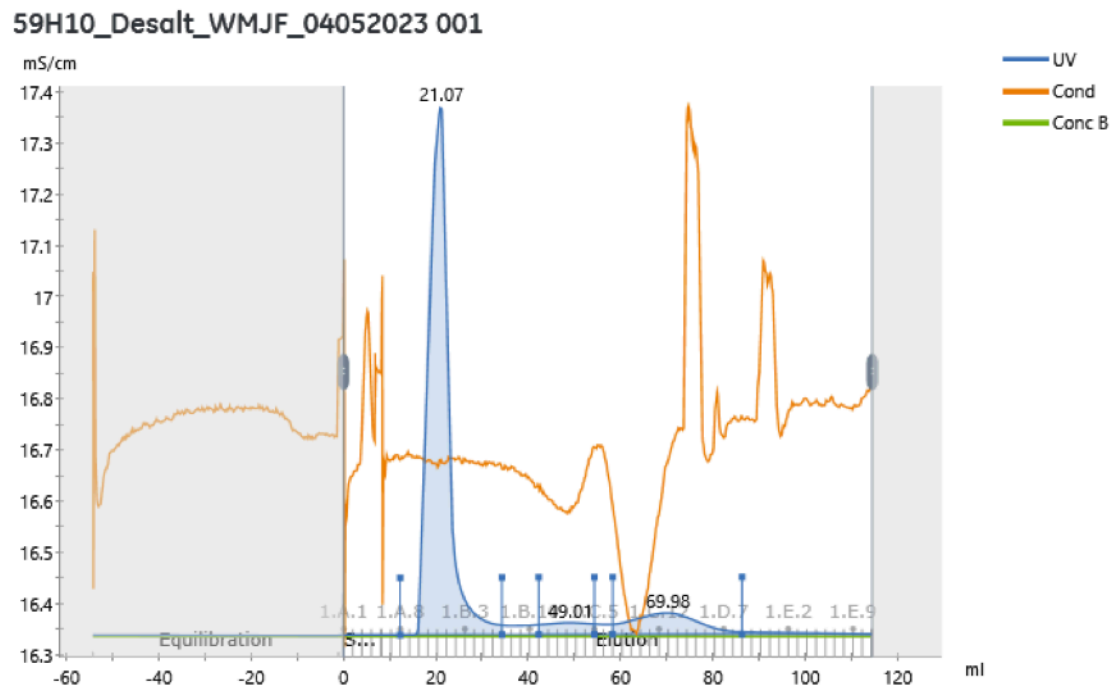


Figure 15: Monitoring of the desalting process using UV recording, where the blue line on the graph represents the absorbance of the nanobody at a specific wavelength. Notably the blue line spikes between collecting columns A8 through B2 (labeled in grey at the bottom). ÄKTA taPure desalting column (Cytiva) was utilized to create this graph.

BLI of 59H10 and HIV-CA121

The Biolayer Interferometry (BLI) assays offer insights into molecular interactions, revealing distinct spectral patterns corresponding to different experimental conditions (figure 16). Within the BLI graph, the dark blue line signifies the nanobody-only control, serving as a reference point to discern the presence of immobilized nanobodies. Conversely, the dark red line depicts the experimental control, showcasing the concurrent presence of both nanobodies and hexamers, thus providing comparative framework to evaluate binding events. The light blue line, in contrast, represents the experimental scenario devoid of immobilized nanobodies, thereby serving as a negative control to ascertain non-specific binding interactions. Each distinct segment of the graph, delineated by dotted lines, corresponds to pivotal experimental phases, delineating the intricate steps of the BLI assay protocol (figure 17).

In the initial segment (0 s to 120 s), characterized by the equilibration phase with buffer alone, minimal fluctuations in wavelengths are observed, establishing a stable baseline for subsequent analyses. Subsequently, the ensuing segment (120 s to 780 s) manifests a discernible increase in wavelength (0.24 nm), which indicates a successful binding of biotinylated nanobodies to the streptavidin-coated sensor surface. As the assay progresses into the subsequent equilibration phase (780 s to 900 s), characterized by buffer alone, the wavelength remains relatively unchanged, substantiating the stability of the system. The introduction of hexamers in the next segment (900 s to 950 s) incites a spike in wavelength (from approximately 0.24 to 0.36 nm), indicative of binding interactions between the nanobodies and hexamers. Additionally, a separate graph with adapted scales illustrates the nanobody baseline (0.24 nm) shifted to 0, with the binding increasing the wavelength to approximately 0.13 nm, further confirming binding events (figure 18). Finally, the last segment (950 s to 1050 s) represents the dissociation phase

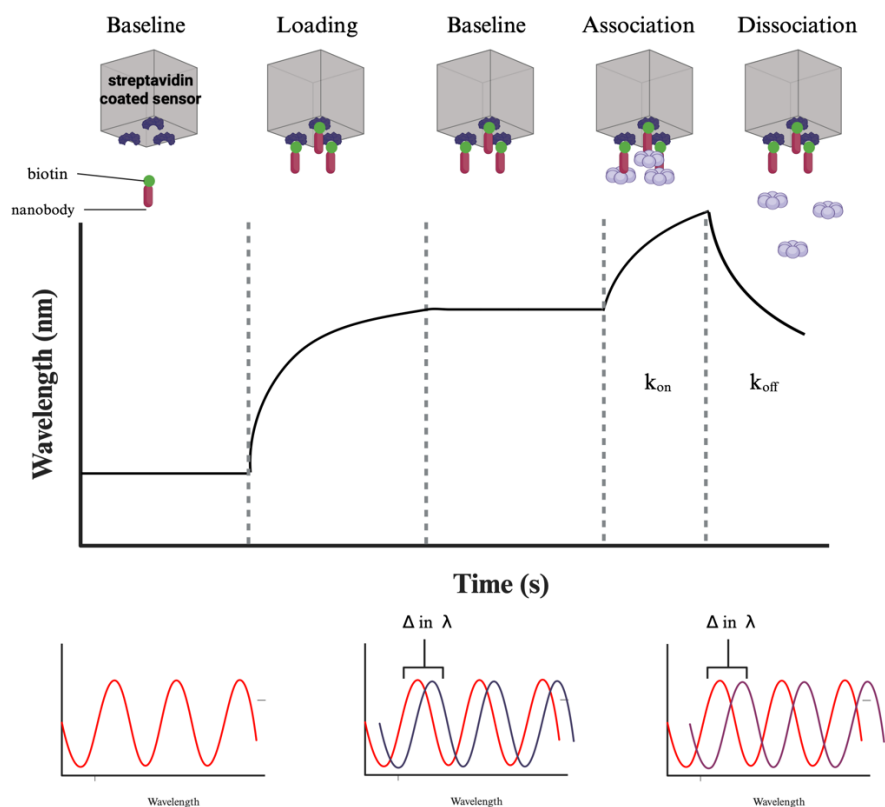


Figure 16: Schematic representation of biolayer interferometry (BLI) methodology. Initially, streptavidin-coated sensors are immersed in a buffer to establish a baseline measurement for wavelength, as light passes through the sensors. Subsequently, biotinylated nanobodies bind to the streptavidin-coated sensors, causing a shift in light wavelength, which is measured relative to the established wavelength baseline. Following this, crosslinked CA hexamers are introduced, resulting in another change in wavelength, which is recorded. Finally, the hexamer assembly is dissociated by immersing the sensors in buffer, allowing for further measurement of wavelength changes. Made with BioRender.com

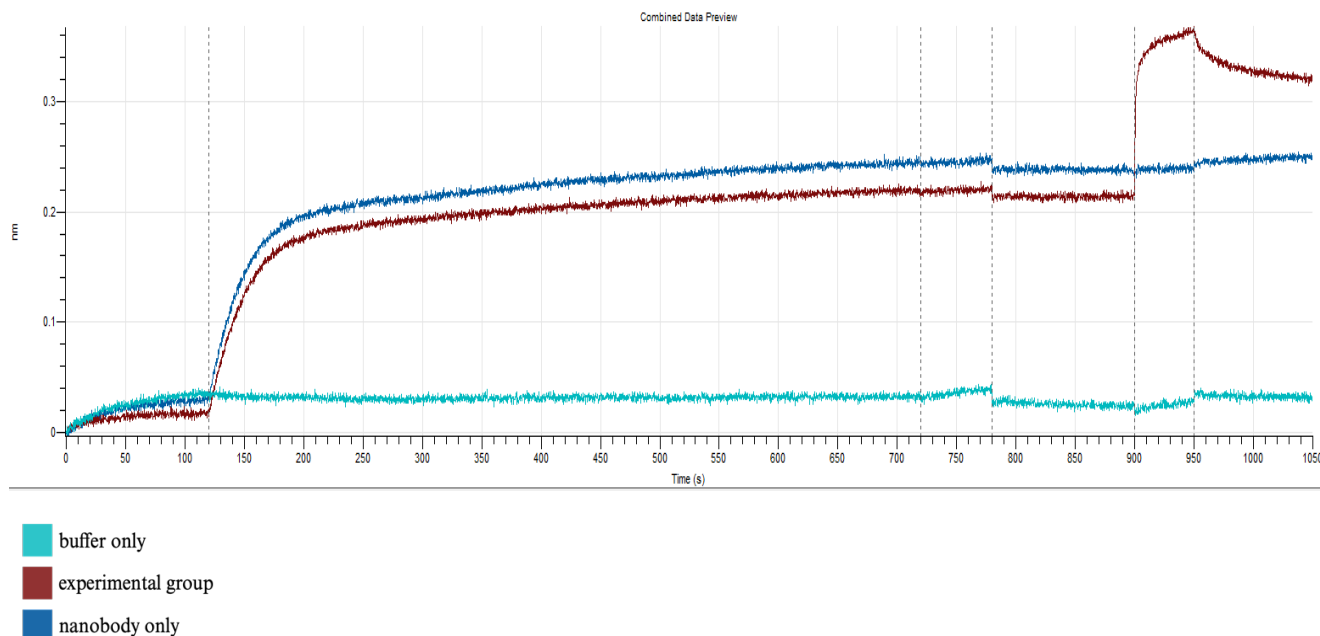


Figure 17: Bio-Layer Interferometry (BLI) graph illustrating the interaction between nanobodies and hexamers, generated using the Sartorius Octet R2 system. The dark blue line represents the nanobody-only control, serving as a reference for immobilized nanobodies. Conversely, the dark red line depicts the experimental group, demonstrating concurrent nanobody and hexamer presence for comparative analysis of binding events. The light blue line serves as a negative control, depicting immobilized nanobodies. Dotted lines delineate distinct segments corresponding to experimental phases, including equilibration with buffer alone, nanobody binding, including equilibration with buffer alone, nanobody binding, subsequent equilibration, hexamer introduction, and dissociation with buffer alone. The graph depicts distinct segments of the assay timeline: equilibration with buffer alone (0 s to 120 s), nanobody binding to streptavidin-coated sensor surface (120 s to 780 s) where the wavelength increased to 0.24 nm, subsequent equilibration with buffer alone (780 s to 900 s), introduction of hexamers (900 s to 950 s) where the wavelength increased to 0.36 nm, and dissociation with buffer alone (950 s to 1050 s) where the wavelength decreased to 0.32 nm.

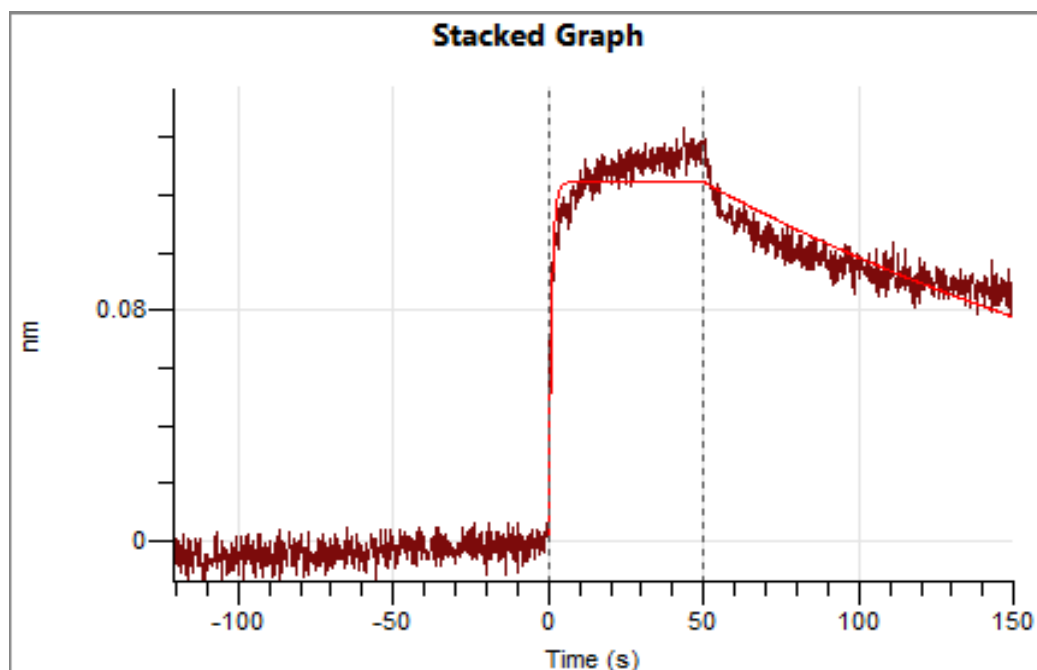


Figure 18: Graph generated using the Sartorius Octet R2 system, adapted from figure 17, illustrating the interaction between nanobodies and the hexamers. The nanobody baseline (0.24 nm) is shifted to 0 on the scale, with binding events causing an increase in wavelength to approximately 0.13 nm.

Index	Color	Sample ID	Conc. (uM)	Response	KD (M)	KD Error	ka (1/Ms)	ka Error	kdis (1/s)
1		CA121	25	0.1339	1.127E-07	6.347E-09	4.189E04	2.245E03	4.722E-03

Table 6: Table displaying kinetic parameters generated using the Sartorius Octet R2 system, including the dissociation constant (K_D) and association constant (k_a). The K_D is measured to be 1.127E-07 (M), while the k_a is determined to be 4.189E04 (1/Ms). Associated errors for both constants are provided.

with buffer alone, showing a slight decrease in wavelength (to about 0.32 nm) (figure 17). The kinetics of binding and dissociation were calculated to determine the dissociation constant (K_D), yielding a value of $1.27E-09$ M, providing insight into the strength of the interaction between the nanobody and its target molecule. In the Gray et al. paper, the 59H10 nanobody binding to the truncated CA monomer had a dissociation constant of $6.9E-10$ M, illustrating a higher binding affinity with the truncated CA monomer in comparison with the hexamer assembly. Furthermore, the association rate constant (k_{on}), calculated to be $4.189E04$ (1/Ms), underscores the rapidity with which binding occurs, further elucidating the dynamic nature of the molecular interactions.

Discussion

The BLI results provide valuable insights into the dynamic interaction between nanobody 59H10 and HIV-1 capsid protein (CA), further elucidating its potential diagnostic and therapeutic applications. The observed binding affinity, with a dissociation constant (K_D) of approximately 112.7 nM, underscores the precise molecular recognition between 59H10 and its target antigen. The BLI data reveals the intricate molecular interface between the nanobody and CA, characterized by multiple hydrogen bond pairs formed between specific residues, particularly R50 and E213 at helix 10 and helix 11 of C-terminal domain of CA (CA_{CTD}), respectively.

Moreover, the observed binding kinetics, with a k_{on} value of 4.189E04 (1/Ms) and k_{off} value of 4.733E-03 (1/s), further corroborate the strong interaction between 59H10 and Capsid hexamers, indicating rapid association and dissociation rates characteristic of stable complex formation. Non-specific aggregation of CA hexamers can hinder the accurate characterization of their structural and functional properties, complicating efforts to decipher mechanisms underlying HIV assembly. The observed binding indicates efficacy in stabilizing these structures, which implies the prevention of undesired aggregate events. The nanobody 59H10 ensures the formation of soluble and well-defined complexes, which are essential for conducting detailed investigations into the interactions between viral components. These interactions play a critical role in various stages of the viral life cycle, including virion assembly, budding, and infectivity.

Moreover, the ability to generate stable hepta-hexamer complexes in the laboratory using the SpyCatcher system opens new avenues for studying HIV assembly dynamics and host-virus interactions.¹³ These complexes serve as valuable tools for elucidating the roles of different viral and cellular factors in shaping the architecture of the HIV capsid lattice. Ultimately, a

comprehensive understanding of CA hexamer assembly and stability is essential for developing novel therapeutic strategies aimed at disrupting viral replication. Therefore, the successful binding of the nanobody 59H10 represents the successful strategy to design tools for studying the HIV-1 capsid with many potential applications planned for future development.

The confirmation of the strong binding of the 59H10 nanobody to the hexamer assembly shows the potential significance as a therapeutic agent against HIV-1. Despite exhibiting a weaker binding affinity compared to the truncated monomer in the Gray et al. paper, the evaluation of its interaction with the hexamer assembly is critical due to its physiological relevance. The hexamer assembly represents the native state of the HIV-1 capsid protein during various stages of the viral life cycle, making it essential to assess the nanobody's efficacy under these conditions. However, to ascertain its specificity, further experiments are warranted. These experiments might include testing the nanobody's binding to other viral or cellular proteins to determine whether its interaction with the hexamer assembly is specific to the CA protein.

Figures

Primer Name	Sequence 5'-3'	T _m °C	CG%	Length (nt)
WM12_59H10_For_OH_pET2 4aVHH	aatgggtcgcggatccgatcaaA TGGCCCAGCTGCAGG AAAG	90.2	57.1	42
WM14_59H10_Rev_OH_pET2 4aVHH_updated	gcccttgctcaccatactagtGCT GCTCACGGTCACC	83.7	59.5	37
WM24_59H10:HA_OH_F	gaaggagatatacatATGGCC CAGCTGCAGG	72	52	31
WM26_59H10_OH_R	ggtggtgctcgagCGCTTGG AAGTACAGGTTTTTCG CTGCTCACGGTCACC	76	60	50

Table 1: Summary of the primers utilized in the cloning process of 59H10:mCherry and 59H10:6xHis. Primers Wm12 and WM14 were employed for cloning the 59H10:mCherry construct, while WM24 and WM26 were utilized for the 59H10:6xHis construct. Properties of each primer, including sequence, melting temperature (T_m), CG content (%), and the length, are all provided. Values were obtained from Snapgene V. 6.0.6.

	Experimental	Primer Control	cDNA Control
(F) WM24	1.25 µL	1.25 µL	-
(R) WM26	1.25 µL	1.25 µL	-
cDNA	0.5 µL	-	0.5 µL
(HF) NEB Phusion	12.5 µL	12.5 µL	12.5 µL
dH₂O	9.5 µL	10 µL	12 µL

Table 2: Overview of the components and amounts used in the PCR process for the preparation of the 59H10 sequence to clone the 59H10:6xHis construct. The table includes quantities of forward and reverse primers, cDNA (59H10 sequence), NEB Phusion mix, dH₂O used in the PCR reaction.

Temperature	Time	Process
98°C	30 seconds	Denaturing
98°C	10 seconds	Annealing
55°C	15 seconds	Annealing
72°C	30 seconds	Annealing
72°C	10 minutes	Extension
4°C	Indefinite	Storage

Table 3: Thermocycler settings employed for the PCR amplification, including denaturation, annealing, extension temperatures, and cycle repetitions. The annealing process was repeated 30 times to ensure optimal primer binding and amplification of the target sequence. The BioRender thermocycler platform was utilized for precise temperature control and cycling parameters.

	Double Digest	NheI Only	XhoI Only	Uncut Control
NheI-HF	2.5 µL	2.5 µL	-	-
XhoI-HF	2.5 µL	-	2.5 µL	-
10x Cutsmart	5 µL	5 µL	5 µL	5 µL
pVHH (5 µg)	25.38 µL	25.38 µL	25.38 µL	5.08 µL
dH₂O	14.62 µL	17.12 µL	17.12 µL	39.92 µL

Table 4: Summary of restriction digestion conditions for excising a 1215-basepair fragment from the pET24a-VHH-mCherry plasmid using NheI and XhoI enzymes, resulting in a fragment size of 52333 basepairs. The table delineates the quantities of enzymes, plasmid DNA, 10x restriction buffer (cutsmart), and dH₂O used for the double digest group, single digest groups with each enzyme separately, and an uncut control.

	1:1 (vector: insert)	1:3 (vector: insert)	1:0 (vector :insert)	0:1 (vector :insert)
pVHH	5 μ L	5 μ L	5 μ L	-
59H10	1.88 μ L	5 μ L	-	1.88 μ L
dH₂O	3.12 μ L	-	5 μ L	8.12 μ L
2X HiFi	10 μ L	10 μ L	10 μ L	10 μ L

Table 5: Assembly of insert (59H10) and plasmid VHH (pVHH) by NEB HiFi assembly with the following amounts and molar ratios. Multiple ratios are tested to increase yield.

References:

- [1] McFadden WM, Snyder AA, Kirby KA, Tedbury PR, Raj M, Wang Z, Sarafianos SG. Rotten to the core: antivirals targeting the HIV-1 capsid core. *Retrovirology*. 2021 Dec 22;18(1):41. doi: 10.1186/s12977-021-00583-z. PMID: 34937567; PMCID: PMC8693499
- [2] Simon V, Ho DD, Abdool Karim Q. HIV/AIDS epidemiology, pathogenesis, prevention, and treatment. *Lancet*. 2006 Aug 5;368(9534):489-504. doi: 10.1016/S0140-6736(06)69157-5. PMID: 16890836; PMCID: PMC2913538.
- [3] Chen B. Molecular Mechanism of HIV-1 Entry. *Trends Microbiol*. 2019 Oct;27(10):878-891. doi: 10.1016/j.tim.2019.06.002. Epub 2019 Jun 28. PMID: 31262533; PMCID: PMC6744290.
- [4] Coffin JM, Hughes SH, Varmus HE, editors. *Retroviruses*. Cold Spring Harbor (NY): Cold Spring Harbor Laboratory Press; 1997. PMID: 21433340.
- [5] Delelis, O., Carayon, K., Saïb, A. *et al.* Integrase and integration: biochemical activities of HIV-1 integrase. *Retrovirology* 5, 114 (2008). <https://doi.org/10.1186/1742-4690-5-114>
- [6] Pancera M, Majeed S, Ban YE, Chen L, Huang CC, Kong L, Kwon YD, Stuckey J, Zhou T, Robinson JE, Schief WR, Sodroski J, Wyatt R, Kwong PD. Structure of HIV-1 gp120 with gp41-interactive region reveals layered envelope architecture and basis of conformational mobility. *Proc Natl Acad Sci U S A*. 2010 Jan 19;107(3):1166-71. doi: 10.1073/pnas.0911004107. Epub 2009 Dec 28. PMID: 20080564; PMCID: PMC2824281.
- [7] Campbell EM, Hope TJ. HIV-1 capsid: the multifaceted key player in HIV-1 infection. *Nat Rev Microbiol*. 2015 Aug;13(8):471-83. doi: 10.1038/nrmicro3503. PMID: 26179359; PMCID: PMC4876022.
- [8] Campbell EM, Hope TJ. HIV-1 capsid: the multifaceted key player in HIV-1 infection. *Nat Rev Microbiol*. 2015 Aug;13(8):471-83. doi: 10.1038/nrmicro3503. PMID: 26179359; PMCID: PMC4876022.
- [9] Ali SA, Teow SY, Omar TC, Khoo AS, Choon TS, Yusoff NM. A Cell Internalizing Antibody Targeting Capsid Protein (p24) Inhibits the Replication of HIV-1 in T Cells Lines and PBMCs: A Proof of Concept Study. *PLoS One*. 2016 Jan 7;11(1):e0145986. doi: 10.1371/journal.pone.0145986. PMID: 26741963; PMCID: PMC4711802.
- [10] Aiken C, Rousso I. The HIV-1 capsid and reverse transcription. *Retrovirology*. 2021 Sep 25;18(1):29. doi: 10.1186/s12977-021-00566-0. PMID: 34563203; PMCID: PMC8466977.
- [11] Bannas P, Hambach J and Koch-Nolte F (2017) Nanobodies and Nanobody-Based Human Heavy Chain Antibodies As Antitumor Therapeutics. *Front. Immunol.* 8:1603. doi: 10.3389/fimmu.2017.01603
- [12] Gray, E. R.; Brookes, J. C.; Caillat, C.; Turbé, V.; Webb, B. L. J.; Granger, L. A.; Miller, B. S.; McCoy, L. E.; El Khattabi, M.; Verrips, C. T. Unravelling the Molecular Basis of High Affinity Nanobodies against HIV p24: *In Vitro* Functional, Structural, and *in Silico* Insights *ACS Infect. Dis.* 2017, 3, 479– 491
- [13] Summers BJ, Digianantonio KM, Smaga SS, Huang PT, Zhou K, Gerber EE, Wang W, Xiong Y. Modular HIV-1 Capsid Assemblies Reveal Diverse Host-Capsid Recognition Mechanisms. *Cell Host Microbe*. 2019 Aug 14;26(2):203-216.e6. doi: 10.1016/j.chom.2019.07.007. PMID: 31415753; PMCID: PMC6777739.

- [14] Zakeri B, Fierer JO, Celik E, Chittock EC, Schwarz-Linek U, Moy VT, Howarth M. Peptide tag forming a rapid covalent bond to a protein, through engineering a bacterial adhesin. *Proc Natl Acad Sci U S A*. 2012 Mar 20;109(12):E690-7. doi: 10.1073/pnas.1115485109. Epub 2012 Feb 24. PMID: 22366317; PMCID: PMC3311370.
- [15] Buser, D. P., Schleicher, K. D., Prescianotto-Baschong, C., & Spiess, M. (2018). A versatile nanobody-based toolkit to analyze retrograde transport from the cell surface. *Proceedings of the National Academy of Sciences*, 115(27), E6227-E6236.
- [16] Alfadhli, A., Romanaggi, C., Barklis, R. L., Merutka, I., Bates, T. A., Tafesse, F. G., and Barklis, E. (2021) Capsid-specific nanobody effects on HIV-1 assembly and infectivity, *Virology* 562, 19-28
- [17] Harmsen MM, De Haard HJ. Properties, production, and applications of camelid single-domain antibody fragments. *Appl Microbiol Biotechnol*. 2007 Nov;77(1):13-22. doi: 10.1007/s00253-007-1142-2. Epub 2007 Aug 18. PMID: 17704915; PMCID: PMC2039825.
- [18] Gres AT, Kirby KA, KewalRamani VN, Tanner JJ, Pornillos O, Sarafianos SG. STRUCTURAL VIROLOGY. X-ray crystal structures of native HIV-1 capsid protein reveal conformational variability. *Science*. 2015 Jul 3;349(6243):99-103. doi: 10.1126/science.aaa5936. Epub 2015 Jun 4. PMID: 26044298; PMCID: PMC4584149.
- [19] McFadden WM, Sarafianos SG. Targeting the HIV-1 and HBV Capsids, an EnCore. *Viruses*. 2023 Mar 31;15(4):896. doi: 10.3390/v15040896. PMID: 37112877; PMCID: PMC10146275.
- [20] “UNAIDS Data 2021.” *UNAIDS*, 2021, www.unaids.org/en/resources/documents/2021/2021_unaids_data.
- [21] Dubrow, A., Zuniga, B., Topo, E., and Cho, J.-H. (2022). Suppressing Nonspecific Binding in Biolayer Interferometry Experiments for Weak Ligand–Analyte Interactions. *ACS Omega* 7, 9206-9211. 10.1021/acsomega.1c05659.